6th International Conference
on
Wind Turbine Noise
Glasgow 20-23 April 2015

Noise Reduction for Small Wind Turbine by Trailing Edge Modification

Takayuki Yamagata, Visualization Research Center, Niigata University, 8050 Ikarashi 2-Nocho, Nishi-ku, Niigata, Japan, yamagata@eng.niigata-u.ac.jp

Nobuyuki Fujisawa, Visualization Research Center, Niigata University, 8050 Ikarashi 2-Nocho, Nishi-ku, Niigata, Japan, fujisawa@eng.niigata-u.ac.jp

Ryo Saito, Faculty of Engineering, Niigata University, 8050 Ikarashi 2-Nocho, Nishi-ku, Niigata, Japan

Summary

Characteristics of discrete tone noise and flow structures are experimentally investigated for flows around NACA0018 airfoils with flatback trailing edges. The velocity fields around the airfoils are measured by particle image velocimetry to understand the relation between the tone noise and the flatback structure. Experimental results indicate that a flatback airfoil with a rounded corner shows comparatively lower peak value of the sound pressure level at small angles of attack. It is found that the velocity fluctuations in the normal component highly correlate with the sound pressure level of the discrete tone noise.

1. Introduction

Noise reduction for small wind turbines is an important topic to minimize a negative influence on people near the wind turbines. One of main causes of the wind turbine noise is discrete tone noise, which is generated from the trailing edge of an airfoil inclined with a small angle of attack to free stream (Arbey and Bataille, 1983; Akishita, 1986; Lee and Lee, 2014). The theory of the trailing edge noise is summarized by Howe (1978). The discrete tone noise is understood as an acoustic field with the self-exited feedback loop between the boundary layer and the wake of the airfoil (Nakano et al., 2007).

In former studies, velocity measurements by particle image velocimetry (PIV) have been carried out for the flow fields around an airfoil to investigate flow structures (Shih et al., 1995; Nakano et al, 2007). According to the experiments, the vortex shedding in the wake and the structure of the boundary layer are highly correlated with the noise emission and noise source distribution (Nakano et al, 2006).

Flow control of the vortex shedding in the wake is effective in order to reduce the discrete tone noise. Several researchers have investigated the flow control techniques such as the active control using a synthetic jet (You and Moin, 2008), the passive controls using an additional rod (Takagi et al., 2006; Greschner et al., 2008),

and a porous material (Hamakawa et al., 2013). Another available technique to control the wake flow is trailing edge modification of the airfoil, which is a passive flow control without additional actuators. In former researches, flow structures behind flatback airfoils with two-dimensional or three-dimensional patterns have been investigated mainly from the viewpoint of the improvement of aerodynamic characteristics and the mechanical strength of the airfoil (Deshpande and Sharma ,2012; Krentel and Nitsche, 2013). However, fewer studies have been reported on the relation between the flatback shape and the tone noise (El-Gammal and Hangan, 2008; Kim et al., 2014).

In this paper, the effect of the trailing edge modification is experimentally investigated for noise reduction of NACA0018 airfoil. The characteristics of the aerodynamic sound noise and velocity fields are measured at various angles of attack.

2. Experimental Methods

2.1 Experimental setup and airfoil shapes

Figure 1 shows an experimental setup for sound pressure and velocity field measurements. The both measurements were carried out in a wind tunnel, which has a closed test section with a cross-section of 190 mm × 190 mm. The test section is placed in an anechoic chamber. Figure 2(a) shows the cross-sectional shape of the NACA0018 airfoil, which has the chord length of C = 80 mm and the spanwise length of 190 mm. The two-dimensional model of the NACA0018 was used in this study as a basic airfoil to investigate the effect of trailing edge modifications. The airfoils are made of resins and are manufactured by 3d printing. The angles of attack for the airfoil were changed from α = 0° to α = 12° by rotating the airfoil. Figure 2(b) shows the cross-sectional shapes of the airfoils with trailing edge modifications. The airfoils of FB-5 and FB-10 have flatback trailing edges and have chord lengths, respectively, 5 mm and 10 mm shortened from that of the NACA0018 airfoil. The airfoil of FB-10RD has a rounded corner at the downside edge of the FB-10 airfoil. Therefore, the only FB-10RD airfoil is an asymmetric shape. Mean velocity of the present experiment was set at U_0 = 30 m/s, which corresponds to Reynolds number Re (= UC/ν, ν is kinetic viscosity) = 1.6 × 10^5 based on the chord length of the basic NACA0018 airfoil. The free-stream turbulence intensity is about 0.8%, which is measured with a hot-wire anemometer.

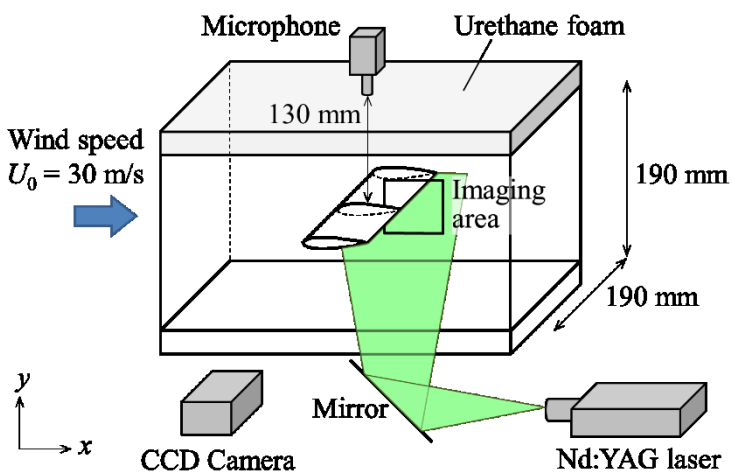

Fig. 1 Experimental setup

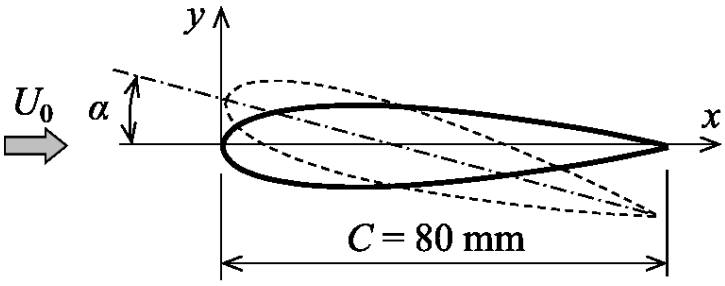

(a) NACA0018

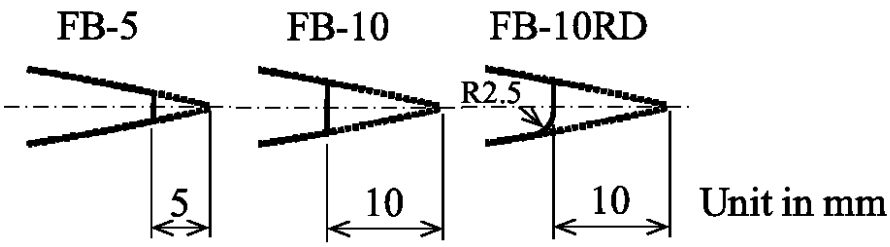

(b) Trailing edge modifications

Fig. 2 Cross-sectional shapes of test airfoils

2.2 Measurement of Sound Pressure Level

Sound pressure levels radiated from the airfoil models were measured by a microphone, which has a diameter of 12.7 mm. The microphone was located above the airfoil with a distance of 130 mm as shown in Fig. 1. The top and bottom walls of the wind tunnel are urethane foam to avoid wind noise, the others are acrylic resin. The sound pressure levels were measured with A-weighting response of the microphone in a range of 20 Hz to 8 kHz, and the sound spectra were measured with a flat frequency response. The output signal of the microphone was recorded with an AD converter. The sampling rate was 10 kHz and the sampling time for statistical evaluation was 10 s. Then the sound spectra were evaluated by FFT analysis of the recorded data.

2.3 Particle Image Velocimetry

In order to elucidate the relation between the sound pressure level and the flow structure, velocity field measurement was carried out by using particle image velocimetry (PIV). The experimental setup for the PIV is shown in Fig. 1. The PIV system used in this study consists of a CCD camera (1280 × 1024, 12 bits) with a flame straddling function, a Nd:YAG laser (100 mJ/pulse), and a pulse generator. The visualizations of the flow fields behind the airfoils were carried out by using oil smoke, which was supplied from a smoke generator. The particle size of the smoke is about 1 μm in diameter. Target areas of the CCD camera was a wake flow region (60 mm × 50 mm) behind the airfoils. PIV analysis was carried out by using a direct cross-correlation algorithm with a sub-pixel interpolation with Gaussian-peak-fitting technique. The maximum pixel displacement of particles was approximately 5 pixels. Therefore, the uncertainty of velocity measurement is estimated as 3%. The sampling rate of the velocity measurement was 4 Hz. The statistical values of the velocity fields were evaluated from 500 instantaneous velocity fields.

3. Results and Discussion

3.1 Sound Pressure Level

Figure 3 shows sound pressure levels of a basic NACA0018 airfoil and airfoils with trailing edge modifications. The sound pressure levels were measured at various angles of attack. The sound pressure level of the NACA0018 airfoil increases at small angles of attack α = 3, 6°, which is due to the generation of the discrete tone noise. Then the sound pressure level decreases at further large angles of attack. These changes for the angles of attack agree well with those of the former research (Nakano et al., 2006). The airfoils of the flatback modification (FB-5 and FB-10) show the peak sound pressure level at different angles of attack from that of NACA0018. The maximum sound pressure levels of FB-5 and FB-10 are the same level as NACA0018 and appear at α = 3° and α = 0°, respectively. Although the FB-10 airfoil shows the high sound pressure level at α = 0°, the sound pressure level at α = 6° is reduced to the same level as the NACA0018 at α = 0°. The flatback airfoil with a rounded corner (FB-10RD) shows a different behaviour of the sound pressure level for the change of the angles of attack. The sound pressure level of FB-10RD at α = 0° is drastically reduced from the flatback airfoil (FB-10), although it is slightly higher than the basic airfoil. The asymmetric airfoil (FB-10RD) keeps low noise emission with increasing angles of attack up to α = 6°. Then the sound pressure level decreases to the same level as the other airfoils.

3.2 Sound Spectrum

Sound spectra of tonal noise for test airfoils were measured for angles of attack α = 0° – 6°. Figure 4(a) shows the sound spectra for the basic airfoil (NACA0018). The sound spectrum at α = 0° has no peak frequency of a noticeable level. Discrete tone noise having a peak frequency of 2 kHz appears with increasing angles of attack. These characteristics of NACA0018 agree well with experimental results in literature (Nakano et al., 2006). The sound spectra for the flatback airfoil (FB-5) are shown in Fig. 4(b). The sound spectrum at α = 0° is similar to that of NACA0018. The strong discrete tone noise appears at α = 3°, having the peak frequency of 2 kHz. At higher angle of attack α = 6°, the peak frequency shifts slightly low frequency side. Figure 4(c) shows the sound spectra for another flatback airfoil (FB-10). The discrete tone

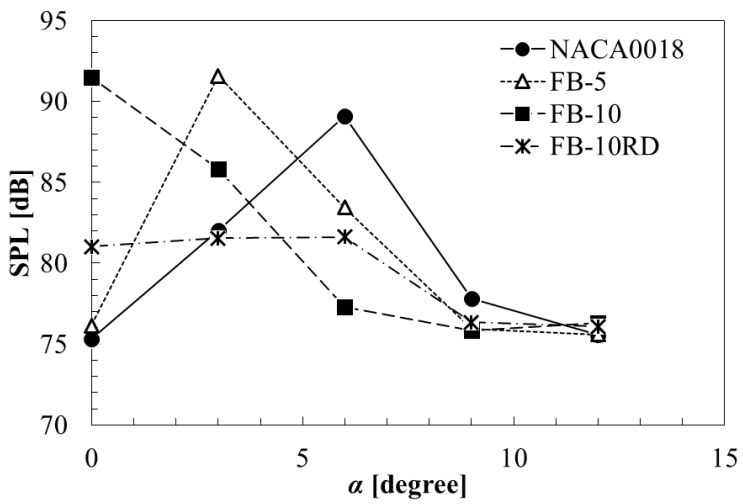

Fig. 3 Sound pressure levels versus angles of attack α

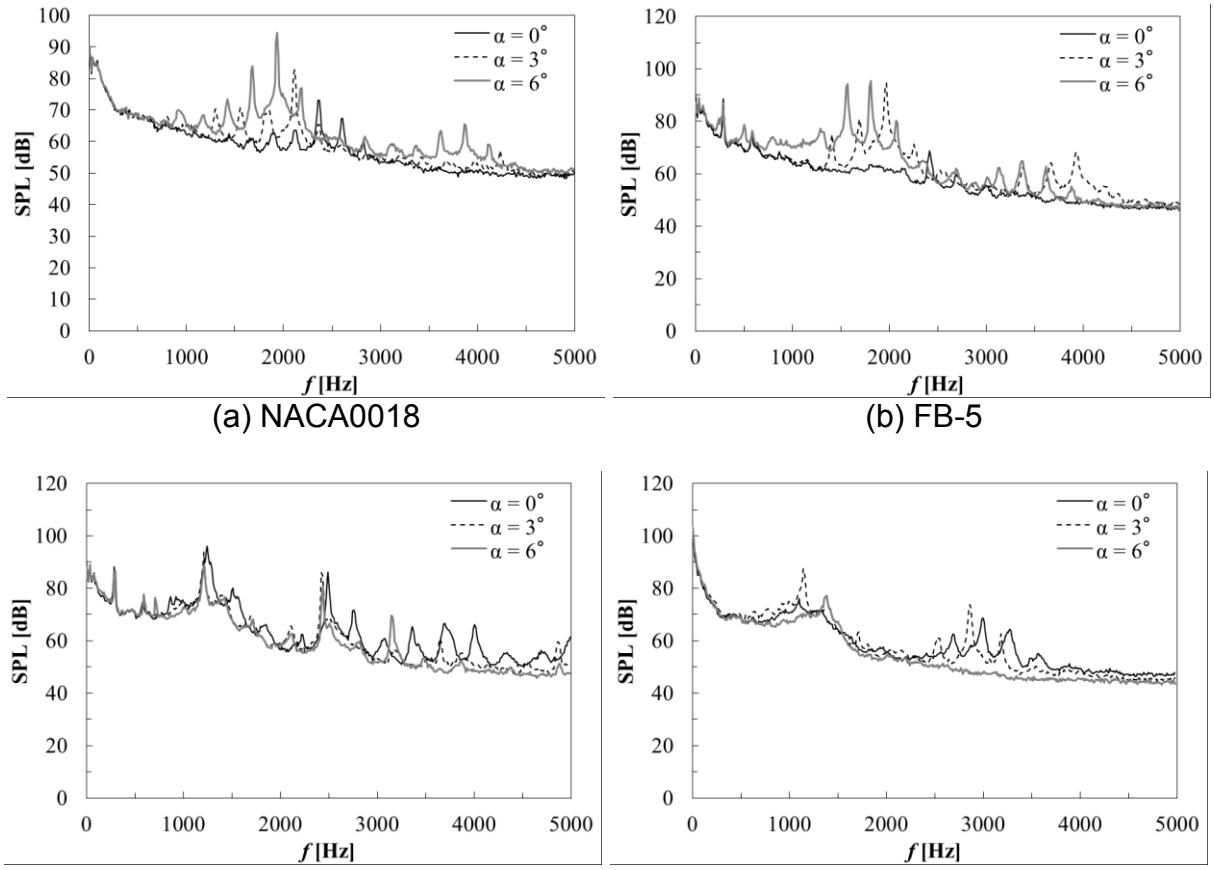

(a) NACA0018 (b) FB-5

(c) FB-10 (d) FB-10RD

Fig. 4 Sound spectrum of tested airfoils

noise is observed at α = 0°, having a peak frequency of 1.2 kHz. The second peak is also observed in the spectrum at the double frequency. Although the discrete tone noise remains with increasing angles of attack, the sound pressure level in higher frequency region decreases. Figure 4(d) shows the sound pressure level for the flatback airfoil with the rounded corner (FB-10RD). The sound spectra have a peak of the tone noise at similar frequency of 1 kHz as the FB-10 airfoil, although the peak levels are reduced. The second peak frequency shits to higher frequency region around 3 kHz.

3.3 Velocity Field

In order to examine the difference in flow structures around airfoils, particle image velocimetry was carried out. Figure 5 shows instantaneous velocity vectors and vorticity contours around the *z*-axis near the trailing edge of the airfoil at α = 0°. The vorticity is defined by $\omega_z = \partial v/\partial x - \partial u/\partial y$ and is normalized by the chord length C and averaged inlet velocity U_0. The instantaneous velocity fields show weak wavy structures downstream of NACA0018 (a) and FB-5 (b), which have low emission of the tone noise in Fig. 3. The positive and negative vorticities are generated from the pressure surface and the suction one, respectively. The vorticity contour of FB-10 (c) shows a strongly wavy structure in which the positive and negative vorticities are alternatively located behind the airfoil. This indicates the vortex generation from the trailing edge, which results in the discrete tone noise emission. In the result of FB-10RD (d), the wavy structure of the vorticity becomes smaller than that of the flatback airfoil FB-10.

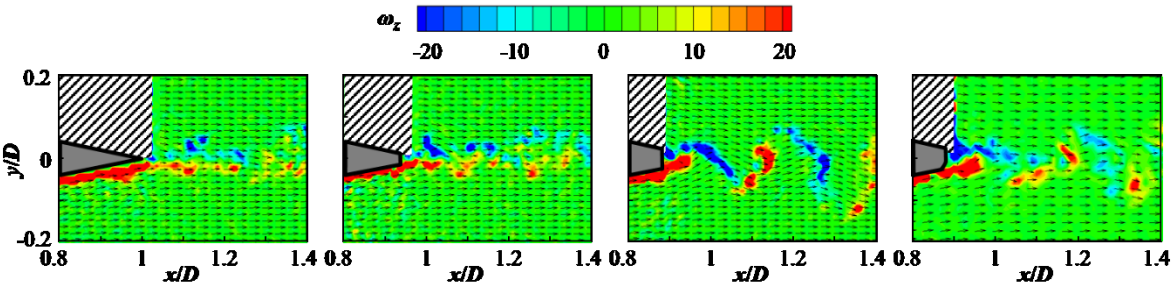

NACA0018 FB-5 FB-10 FB-10RD

Fig. 5 Instantaneous velocity fields behind airfoils (α = 0°)

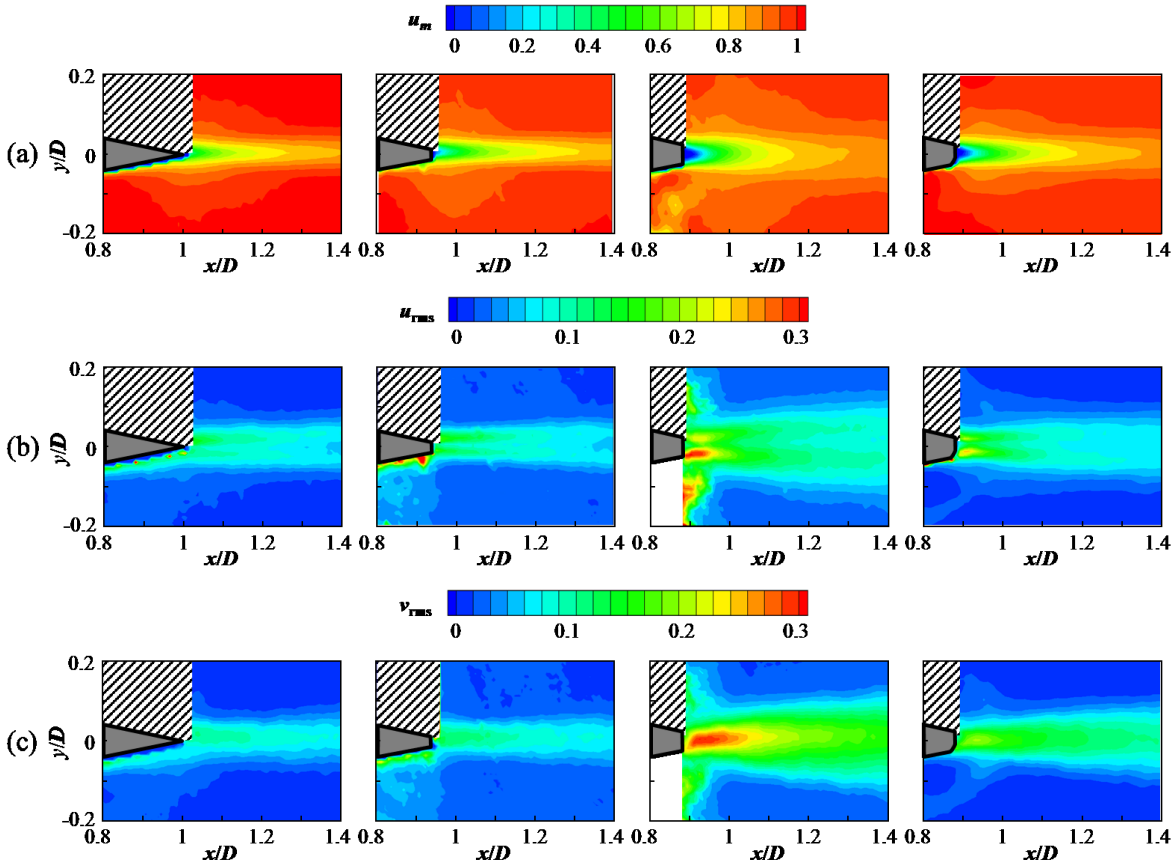

NACA0018 FB-5 FB-10 FB-10RD

Fig. 6 Statistical velocity fields behind airfoils (α = 0°): (a) streamwise mean velocity, (b) streamwise velocity fluctuation, (c) normal velocity fluctuation

Figure 6 shows statistical velocity fields at α = 0°for test airfoils: NACA0018, FB-5, FB-10, and FB-10RD. Figure 6(a) illustrates the streamwise mean velocity contours around trailing edge. The NACA0018 and FB-5 airfoils show narrow wake flow behind the airfoils. In the result of the FB-10 airfoil, a stagnant flow region is seen behind the flatback surface. Moreover, the wake flow of the FB-10 becomes wider than that of the former airfoils. The FB-10RD airfoil shows the narrow wake flow, though the stagnant flow region occurred behind the airfoil.

Figures 6(b) and 6(c) show the streamwise and normal velocity fluctuation contours, respectively. The velocity fluctuations of NACA0018 and FB-5 show low turbulence level in the wake flow. The FB-10 airfoil shows the high turbulence level in

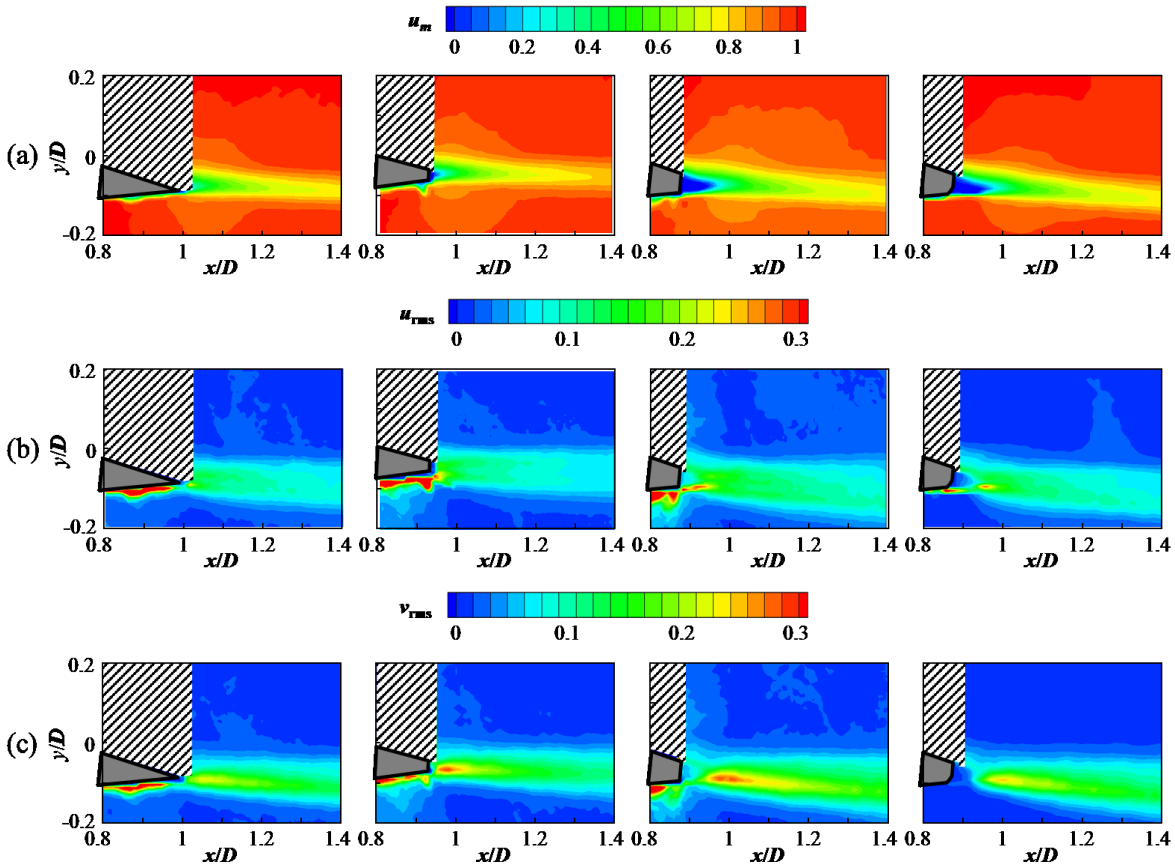

NACA0018 FB-5 (α = 3°) FB-10 FB-10RD

Fig. 7 Statistical velocity fields behind airfoils (α = 6°): (a) streamwise mean velocity, (b) streamwise velocity fluctuation, (c) normal velocity fluctuation

the streamwise and normal velocity fluctuations. Therefore, the FB-10 airfoil has the large noise emission at α = 0°. The FB-10RD airfoil shows wide wake region, while the peak fluctuation in the normal component is reduced by comparing to the FB-10 airfoil.

Figure 7 shows the statistical velocity fields at α = 6° for test airfoils. Note that the results for the FB-5 airfoil are those at α = 3°, because the FB-5 airfoil has the maximum sound pressure level at the angle. Figure 7(a) compares streamwise mean velocity contours around the trailing edge. It is seen that wake region on the suction surface side becomes wider than that on the pressure surface side in the results of NACA0018 and FB-5. This implies deceleration of flow on the suction side due to turbulence production. In the result of FB-10, the wake flow shows sharp distributions similar to the former airfoils. The mean velocity field of FB-10RD is similar to that of FB-10.

Figures 7(b) and 7(c) show the streamwise and normal velocity fluctuation contours, respectively. In the results of NACA0018, the turbulent region on the suction side grows wider than that on the pressure side, while the strong velocity fluctuation occurs in the normal velocity component on the pressure side. The FB-5 airfoil shows the same pattern as the NACA0018 at the increased angle of attack. In the result of FB-10, the high velocity fluctuation is generated in the normal component, though the position is away from the flatback surface. The spread of the wake region with high velocity fluctuations is constricted in comparison with that at α

= 0°. The FB-10RD airfoil also shows the low turbulence level in the normal velocity component. Moreover, the velocity fluctuation near the rounded corner decreases appreciably. This implies the flow separation on the pressure side is changed for the FB-10RD airfoil, which relates to the vortex shedding and the tone noise emission.

Conclusions

In this study, the effect of the trailing edge modification was experimentally investigated for the discrete tone noise emission of the NACA0018 airfoil. The sound pressure levels radiated from a basic airfoil and airfoils with flatback trailing edge with and without rounded corner were measured by a microphone at several angles of attack. Flow structures around the trailing edge of the airfoils were measured by PIV. As the results, the flatback airfoil with a rounded corner showed comparatively lower peak value of the sound pressure level at angles of attack between 0° to 12°. The velocity fluctuations in the normal component were highly correlated with the sound pressure level of the discrete tone noise.

References

Akishita S (1986) Tone-like noise from an isolated two dimensional airfoil, AIAA paper, 86-1947.

Arbey H and Bataille J (1983) Noise generated by airfoil profiles placed in a uniform laminar flow, J. Fluid Mech., 134, 33-47.

Deshpande PJ and Sharma SD (2012) Spanwise vortex dislocation in the wake of segmented blunt trailing edge, J. Fluids Struct., 34, 202-217.

El-Gammal M and Hangan H (2008) Three-dimensional wake dynamics of a blunt and divergent trailing edge airfoil, Exp. Fluids, 44, 705-717.

Greschner B, Thiele F, Jacob MC and Casalino D (2008) Prediction of sound generated by a rod-airfoil configuration using EASM DES and the generalised Lighthill/FW-H analogy, Comp. Fluids, 37, 402-413.

Hamakawa H, Hosokai K, Adachi T and Kurihara E (2013) Aerodynamic sound radiated from two-dimensional airfoil with local porous material, Open J. Fluid Dyn., 3, 55-60.

Howe MS (1978) A review of the theory of trailing-edge noise, J. Sound Vib., 61, 437-465.

Kim T, Jeon M, Lee S Shin H (2014) Numerical simulation of flatback airfoil aerodynamic noise, Renewable Energy, 65, 192-201.

Krentel D and Nitsche W (2013) Investigation of the near and far wake of a bluff airfoil model with trailing edge modifications uxing time-resolved particle image velcimetry, Exp. Fluids, 54, 1551 (16 pages).

Lee S and Lee S (2014) Numerical and experimental study of aerodynamic noise by a small wind turbine, Renewable Energy, 65, 108-112.

Nakano T, Fujisawa N and Lee S (2006) Measurement of tonal-noise characteristics and periodic flow structure around NACA0018 airfoil, Exp. Fluids, 40, 482-490.

Nakano T, Fujisawa N, Oguma Y, Takagi Y and Lee S (2007) Experimental study on flow and noise characteristics of NACA0018 airfoil, J. Wind Eng. Indust. Aerod., 95, 511-531.

Shih C, Lourenco L and Krothapalli A (1995) Investigation of flow at leading and trailing edges of pitching-up airfoil, AIAA J., 33, 1369-1376.

Takagi Y, Fujisawa N, Nakano T and Nashimoto A (2006) Cylinder wake influence on the tonal noise and aerodynamic characteristics of a NACA0018 airfoil, J. Sound Vib., 297, 563-577.

You D and Moin P (2008) Active control of flow separation over an airfoil using synthetic jets, J. Fluids Struct., 24, 1349-1357.